Single-Molecule Microscopy Reveals Dynamic FLNA Interactions Governing SSTR2 Clustering and Internalization

Treppiedi, D; Jobin, Marie-Lise; Peverelli, Erika; Giardino, E; Sungkaworn, Titiwat; Zabel, Ulrike; Arosio, Maura; Spada, Anna; Mantovani, Giovanna; Calebiro, Davide

DOI:
https://doi.org/10.1210/en.2018-00368

Single-Molecule Microscopy Reveals Dynamic FLNA Interactions Governing SSTR2 Clustering and Internalization

Donatella Treppiedi[1*], Marie-Lise Jobin[2], Erika Peverelli[1], Elena Giardino[1], Titiwat Sungkaworn[2], Ulrike Zabel[2], Maura Arosio[1], Anna Spada[1], Giovanna Mantovani[1†*], Davide Calebiro[2,3,4†*]

Author affiliations

[1] Endocrine Unit, Fondazione IRCCS Ca' Granda Ospedale Maggiore Policlinico; Department of Clinical Sciences and Community Health, University of Milan, 20122 Milan, Italy.

[2] Institute for Pharmacology and Toxicology, University of Würzburg, and Bio-Imaging Center/Rudolf Virchow Center, University of Würzburg, 97078 Würzburg, Germany.

[3] Institute of Metabolism and Systems Research, University of Birmingham, B15 2TT Birmingham, UK.

[4] Centre of Membrane Proteins and Receptors (COMPARE), Universities of Birmingham and Nottingham, UK.

* To whom correspondence should be addressed:

Donatella Treppiedi

Endocrine Unit, Fondazione IRCCS Ca' Granda Ospedale Maggiore Policlinico; Department of Clinical Sciences and Community Health, University of Milan.

Via F. Sforza, 35

20122-Milan, Italy

Phone +39 02 55033512

Fax +39 02 55033361

E-mail: donatella.treppiedi@unimi.it

Giovanna Mantovani

Endocrine Unit, Fondazione IRCCS Ca' Granda Ospedale Maggiore Policlinico; Department of Clinical Sciences and Community Health, University of Milan.

Via F. Sforza, 35

20122-Milan, Italy

Phone +39 02 55033481

E-mail: giovanna.mantovani@unimi.it

Davide Calebiro

Institute of Pharmacology and Toxicology, University of Würzburg, and Bio-Imaging Center/Rudolf Virchow Center, University of Würzburg, 97078 Würzburg, Germany; Institute of Metabolism and Systems Research, University of Birmingham, B15 2TT Birmingham, UK; Centre of Membrane Proteins and Receptors (COMPARE), Universities of Birmingham and Nottingham, UK.

Phone +44 1214143928

E-mail: D.Calebiro@bham.ac.uk

† G. M. and D. C. should be both considered as last author

Disclosure: The authors declare that they have no conflict of interests.

Abstract

The cytoskeletal protein filamin A (FLNA) has been suggested to play an important role in the responsiveness of GH-secreting pituitary tumors to somatostatin receptor subtype 2 (SSTR2) agonists, by regulating SSTR2 expression and signaling. However, the underlying mechanisms are unknown. Here, we use fast multi-color single-molecule microscopy to image individual SSTR2 and FLNA molecules at the surface of living cells with unprecedented spatiotemporal resolution. We find that SSTR2 and FLNA undergo transient interactions, which occur preferentially along actin fibers and contribute to restraining SSTR2 diffusion. Agonist stimulation increases the localization of SSTR2 along actin fibers and, subsequently, SSTR2 clustering and recruitment to clathrin-coated pits (CCPs). Interfering with FLNA–SSTR2 binding with a dominant-negative FLNA fragment increases SSTR2 mobility, hampers the formation and alignment of SSTR2 clusters along actin fibers, and impairs both SSTR2 recruitment to CCPs and SSTR2 internalization. These findings indicate that dynamic SSTR2–FLNA interactions critically control the nanoscale localization of SSTR2 at the plasma membrane and are required for coupling SST2R clustering to internalization. These mechanisms explain the critical role of FLNA in the control of SST2R expression and signaling and suggest the possibility of targeting SSTR2–FLNA interactions for the therapy of pharmacologically resistant GH-secreting pituitary tumors.

Keywords: Scaffolding proteins; cytoskeleton; GPCR endocytosis; TIRF microscopy

1. Introduction

Somatostatin (SS) is a peptide hormone that exerts key regulatory functions on the endocrine, neuronal and gastrointestinal systems. These actions are mediated by a family of five G-protein-coupled receptors (GPCRs) known as SSTR1–5 (1, 2), and include inhibition of both cell proliferation and hormone secretion (3–6). Somatostatin receptor type 2 (SSTR2) – one of the most expressed receptor subtypes in GH-secreting pituitary adenomas – is the main target of somatostatin analogs (SSAs), which are widely used to treat acromegalic patients (7, 8). However, a relevant subset of patients is not successfully controlled by medical therapy with SSAs (9–11), and several studies have attempted to clarify the molecular mechanisms underlying the pharmacological resistance to SSAs (12–15). More recently, increasing attention has been directed towards the role of scaffolding proteins and cytoskeletal elements in mediating the formation of specialized signaling subdomains at the plasma membrane and facilitating receptor internalization (16–19). Thus, a better understanding of these mechanisms appears crucial to develop innovative pharmacological therapies for acromegaly and other human diseases.

Filamin A (FLNA) is a large cytoskeletal protein characterized by an actin binding domain located at its N-terminus and multiple binding sites for molecules involved in different signaling pathways, which are distributed along the rest of its flexible structure. The primary function of FLNA is to cross-link actin filaments (F-actin) into a three-dimensional network that defines and controls cell shape. In addition, thanks to its ability to anchor transmembrane proteins to the actin cytoskeleton and its scaffolding role for intracellular proteins, FLNA is emerging as an important regulator of G-coupled receptor (GPCR) expression, subcellular localization, trafficking and signaling (20, 21). In particular, previous studies suggested that FLNA directly interacts with SSTR2 and that this interaction might be required for the SSTR2-mediated biological effects of

SSAs (17, 22). However, how these interactions affect SSTR2 organization at the plasma membrane and its internalization was unknown.

Here, we used innovative single-molecule imaging methods based on total internal reflection fluorescence (TIRF) microscopy (23-26) to investigate the involvement of FLNA in the spatial arrangement, mobility and internalization of SSTR2s with unprecedented spatio-temporal resolution. Our findings indicate that FLNA plays an important role in controlling the arrangement and mobility of SSTR2s at the plasma membrane by providing a physical link with actin fibers, which facilitates the clathrin-mediated internalization of SSTR2s.

2. Materials and Methods

Plasmids and constructs

A plasmid encoding the human wild-type SSTR2 was kindly provided by Dr. Stefan Schulz. A plasmid encoding the SSTR2 with a FLAG sequence followed by a SNAP tag at its N-terminus (SNAP-SSTR2) was cloned by inserting the SSTR2 receptor sequence into a plasmid containing the SNAP tag directly after the FLAG sequence (23). A plasmid encoding FLNA with a CLIP tag inserted in its first hinge region (CLIP-FLNA) was generated by replacing eGFP with a CLIP tag in a construct coding for eGFP-FLNA (27), kindly provided by Dr. Anna M. Aragay. Plasmids expressing the FLNA repeats 19-20 or 17-18 (FLNA 19-20, FLNA 17-18) were previously described (17). A plasmid encoding eGFP-AP2 (28) was kindly provided by Dr. Emanuele Cocucci and Dr. Tom Kirchhausen. The plasmid coding for LifeAct-GFP (29) was kindly provided by Prof. Antje Gohla (Institute for Pharmacology and Toxicology, University of Würzburg).

Cell culture

Chinese hamster ovary K1 (CHO-K1) cells were maintained in Dulbecco's modified Eagle's medium/nutrient mixture F-12 (DMEM/F12) supplemented with 10% (v/v) fetal bovine serum (FBS), 100 U/ml penicillin and 100 µg streptomycin. Human embryonic kidney 293A (HEK293A) cells were grown in Dulbecco's modified Eagle's medium (DMEM) supplemented with 10% (v/v) FBS, 2mM glutamine, 100 U/ml penicillin and 100 µg streptomycin. Cells were maintained in a humidified atmosphere of 5% CO_2 at 37 °C.

cAMP measurements

To assess the functionality of the SNAP-SSTR2 construct, HEK293A cells were transiently cotransfected for 48 h with 1 µg of wild-type or SNAP-tagged SSTR2 and 1 µg of a fluorescence resonance energy transfer (FRET) sensor for cAMP (Epac1-camps) (30, 31) using the Effectene reagent (QIAgen, Hilden, Germany), and according to the instructions of the manufacturer. Ratiometric FRET measurements of intracellular cAMP levels, before and after incubation with increasing concentration of the selective SSTR2 agonist BIM23120 (Ypsen, Milan, IT), were performed on an Axiovert 200 inverted microscope (Zeiss; Jena, Germany), equipped with an oil-immersion objective (plan-NEOFLUAR 63×/1.25), a 505 dcxr beam splitter (Visitron Systems; Puchheim, Germany), a high-speed polychromator system (Visitron Systems) and an iXon Ultra EMCCD camera (Andor; Belfast, UK) (32).

Total Internal Reflection Fluorescence Microscopy

For single-molecule experiments, CHO cells were seeded on 24-mm clean glass coverslips at a density of 3×10^5 cells per well, in complete phenol-red-free medium in order to minimize autofluorescence. On the following day, cells were transiently transfected with 2 µg DNA and 4-6 µL of Lipofectamine 2000 transfection reagent (Invitrogen, Carlsbad, CA), according to the manufacturer´s instructions. Cells were analyzed 4–12 h after transfection to achieve low

expression levels. CHO cells, transfected with SNAP-SSTR2 and CLIP–FLNA were labeled with 1 μM Alexa647-BG (Alexa Fluor 647-SNAP Surface; New England Biolabs, UK) and 1 μMTMR-BC (CLIP-Cell TMR-Star; New England Biolabs, UK), respectively. Labeling was performed in complete phenol-red-free medium for 20 min at 37 °C 5% CO_2. At the end of the incubation, cells were washed three times with complete phenol-red-free medium, each time followed by 5 min incubation at 37 °C, and immediately imaged. These conditions resulted in optimized labeling of cell-surface SNAP-tagged receptors and intracellular CLIP-FLNA particles. A custom total internal reflection fluorescence (TIRF) microscope based on an Eclipse Ti (Nikon) equipped with four EMCCD cameras (iXon DU897, Andor), 405 nm, 488 nm , 561 nm and 640 nm diode lasers (Coherent), and a 100× oil-immersion objective (CFI Apo TIRF 100x N.A. 1.49, Nikon) was used. Cells were first searched using bright field illumination and then a fine focus adjustment was performed switching to TIRF mode, always keeping the intensity of the laser power as low as possible (3% laser power). This procedure minimized photobleaching before image acquisition. Afterwards, laser power was set to 30% and image sequences (300–400 frames) were acquired with an exposure time of 30 ms, resulting in an interval between frames of 61.9 ms. The penetration depth of the evanescent field was ~100 nm. The microscope was equipped with an incubator and a temperature control unit. Experiments were performed at 20.5 ± 0.3 °C. Only cells with less than 0.57 receptor particle/μm^2 were analyzed.

MSD analysis

Single-molecule image sequences were analyzed as previously described (23–26), including automated single particle detection and tracking, which were performed using the *utrack* software in MATLAB (MathWorks) environment (33). Receptor diffusion was calculated on the basis of a

mean square displacement (MSD) analysis of individual trajectories derived from TIRF image sequences as previously described (24). MSD data were fitted with the following equation:

$$MSD\ (t) = 4Dt^{\alpha} + 4{\sigma_l}^2 \quad \text{(Eq. 1)}$$

where t indicates time and α is the anomalous diffusion exponent. σ_l is the standard deviation of the localization error, which was estimated to be approximately 23 nm. Only trajectories lasting at least 70 frames were analyzed. Since this analysis revealed heterogeneity among particles, trajectories were then classified according to the diffusion parameters D and α. We considered particles with $D < 0.01\ \mu m^2.s^{-1}$ to be confined. Particles with $D \geq 0.01\ \mu m^2.s^{-1}$ and $0.75 \leq \alpha \leq 1.25$ were considered to have normal diffusion. Particles were considered to have sub- or super-diffusion in case of $D \geq 0.01\ \mu m^2.s^{-1}$ and $\alpha < 0.75$ or $\alpha > 1.25$, respectively.

Colocalization index analysis based on single-molecule localizations

To analyze the relationship between localizations of SSTR2 obtained by single-molecule microscopy and the signals obtained in the actin channel, we adapted the method developed by Ibach et al. (34), as previously described (26). The method is based on a modification of Manders´ colocalization coefficients (35). Briefly, in our study, we generated a binary mask corresponding to the fibers the actin channel and we calculated the number of SSTR2 localizations where the mask in the actin channel is equal to 1. This was used to calculate a colocalization index, whose values can range from -1 in case of perfect anti-correlation to +1 in case of perfect correlation/colocalization, whereas a value of 0 indicates no colocalization.

Immunofluorescence and confocal fluorescence microscopy

CHO cells were plated on 13-mm coverslips at a density of 1.5×10^5 cells per well in 24-well plates and grown at 37 °C for 18 h. Cells were then cotransfected with LifeAct-GFP, SNAP-

SSTR2 and FLNA17-18 or FLNA19-20. Receptors were labeled 24-48 h after transfection and stimulated with saturating concentration (100 nM) of BIM23120 up to 10 min to observe receptor clusters alignment with actin and colocalization with AP-2, for 15, 30, and 60 min to follow receptor internalization, at 37°C. After that, cells were fixed with 4% paraformaldehyde for 10 min at room temperature, and washed three times in PBS. Cells cotransfected with SNAP-SSTR2 and FLNA fragments only were permeabilized with 0.3% Triton X-100 in PBS for 5 min, incubated with 10% FBS in PBS (Thermofisher, Rockfor, IL) for 30 min and then incubated with anti AP-2 antibody (Thermofisher, Rockfor, IL) for 2 h at room temperature. After 3 washes with PBS containing 0.05% Tween 20, cells were stained with Alexa Fluor 488 conjugated secondary antibody (Thermofisher, Rockfor, IL) for 1 h at room temperature and extensively washed. Both primary and secondary antibodies were diluted in an antibody dilution buffer containing 1% BSA, 0.3% Triton X-100 in PBS. All coverslips were mounted on glass slides with ProLong Diamond Antifade mounting medium with 4',6-diamidino-2-phenylindole (DAPI) (Life Technologies, Carlsbad, CA). Image acquisition was performed on a Leica TCS SP2 laser scanning confocal microscope equipped with Ar 488 nm, HeNe 543 nm and 635 nm lines and a 63× objective (HCX PL APO 63X/1.4-0.60 OIL) (Leica Microsystems, Wetzlar, Germany).

Colocalization analysis based on confocal images

For colocalization analysis based on confocal microscopy, confocal images in the different channels were acquired separately, upon adjusting the photomultiplier gain for each channel to minimize background noise and avoid saturated pixels. Only the optical section corresponding to the plasma membrane was analyzed. The degree of colocalization between SSTR2 and actin and between SSTR2 and AP-2 were measured on raw images, by calculating Pearson's correlation coefficient (PCC) and Manders' colocalization coefficients (MCC), respectively, with the JACoP

tool in the NIH ImageJ software. SSTR2 clusters analysis was performed by including clusters of area between 0.01 and 0.3 μm^2.

Quantification of SSTR2 internalization

To quantify SSTR2 internalization, about 8-12 equatorial confocal sections from each cell body were sequentially collected to ensure a scan thickness of ~ 500 nm. The mean fluorescence density (*F*) in two distinct regions corresponding to the plasma membrane and the cytosol were determined densitometrically in one representative focal plane for each cell. The mean plasma membrane to cytosol fluorescence ratio (f_R) was then calculated according to the following equation: f_R = [*F*(membrane) - *F(*background)] / [*F*(total) - *F*(background)] with NIH ImageJ, as previously described (36). At least 30 cells for each group, from three independent transfections were analyzed, and results were plotted as mean value ± SEM expressed as % of basal condition.

An assay based on reversible biotinylation of cell surface-proteins was used to quantify receptor internalization. CHO cells transiently expressing FLNA fragments and wild-type SSTR2 were washed three times with ice-cold PBS, followed by a 30-min incubation with 500 µg/ml cleavable EZ-Link sulfo-NHS-SS-biotin (Thermofisher, Rockfor, IL) at 4 °C. Unreacted biotin was blocked and removed by three washes with cold Tris-buffered saline containing 10 mM glycine. Biotinylated cells were incubated in pre-warmed medium with or without 100 nM BIM23120 at 37 °C for 30 min, and then chilled on ice to stop endocytosis. Glutathione (Sigma-Aldrich, St. Louis, MO) was used to release the biotin label from proteins at the cell surface: cells were washed twice with cold glutathione strip buffer (50 mM glutathione, 75 mM NaCl, 75 mM NaOH, 10% FBS in H_2O), at 4 °C for 20 min. Excess glutathione was then quenched by 30 min incubation with 50 mM iodoacetamide (Sigma-Aldrich, St. Louis, MO) in PBS, 1% BSA, pH 7.4 at 4 °C. Cells were lysed with 35 µl lysis buffer (Cell Signaling Technology, Danvers, MA) and

60 µg of total cellular protein extract was incubated with 1 µg SSTR2 (yI-17) antibody (Santa Cruz Biotechnology, Santa Cruz, CA) in a total volume of 100 µl of lysis buffer over night at 4 °C on a rotating device, for immunoprecipitation. 20 µl of protein A/G Plus-Agarose (Santa Cruz Biotechnology, Santa Cruz, CA) was then added, and tubes were incubated for 3 h at 4 °C under constant rotation. After 5 washes with ice-cold PBS, the pellet was resuspended in 45 µl of Blue loading buffer (Cell Signaling Technology, Danvers, MA). Eluted proteins were separated by SDS-PAGE under nonreducing conditions. To detect biotinylated proteins, a 1:500 dilution of a horseradish peroxidase-linked antibody specific for biotin (Cell Signaling Technology, Danvers, MA) was used. The presence of equal receptor amounts in the immunoprecipitates was confirmed by stripping and reprobing with an antibody against SSTR2 (1:1000; UMB-1, Abcam, Cambridge, UK) and using an anti-mouse secondary antibody covalently coupled to horseradish peroxidase (1:2000). The resulting bands were analyzed with the NIH ImageJ software. Experiments were performed in triplicate.

Statistical analysis

All statistical analyses were performed using the Prism 7 software (GraphPad, San Diego, CA). Unless otherwise stated, data were analyzed by two-tailed paired Student *t* test or Chi square test, as indicated. $P < 0.05$ was accepted as statistically significant.

3. Results

Single-molecule microscopy captures individual SSTR2 and FLNA molecules in living cells

To visualize individual SSTR2 molecules at the plasma membrane of living cells, we generated a SSTR2 construct carrying a SNAP-tag at its N-terminus (SNAP-SSTR2) (37). The functional activity of SNAP-SSTR2 was confirmed by testing its ability to inhibit adenylyl cyclase activity

in transfected HEK293A cells incubated with increasing concentrations of the selective SSTR2 agonist BIM23120 (Figure 1A and Supplemental Fig. 1). To allow simultaneous imaging of SSTR2 and FLNA, we additionally generated a FLNA construct carrying a CLIP-tag within its first hinge region (CLIP-FLNA) (Figure 1B) (38). The CLIP-FLNA construct was validated in transfected CHO cells for its capacity to induce correct stress fibers organization and colocalize with actin filaments (Supplemental Fig. 2). These constructs were subsequently transiently transfected in CHO cells, covalently labeled with selective SNAP and/or CLIP fluorescent substrates and imaged by fast one- or two-color TIRF microscopy (Figure 1C, D). Individual SSTR2 and FLNA particles were then automatically detected and tracked using the *utrack* software (33) (Figure 1E, F, G, H).

Single-molecule analysis of SSTR2 reveals heterogeneous receptor dynamics at the plasma membrane

The spatio-temporal dynamics of SSTR2 at the plasma membrane of living cells was first analyzed in terms of receptor lateral mobility. To this end, CHO cells, which do not express endogenous SSTR2 (data not shown), were transiently transfected to express SNAP-SSTR2 at low physiological densities (0.57 ± 0.07 particle/μm^2) and imaged by TIRF microscopy before and up to 5 min after stimulation with 100 nM of BIM23120. A mean-square displacement (MSD) analysis (23, 26) was used to estimate the diffusion coefficients of the SSTR2 particles based on their trajectories (Figure 2A and B). The results of this analysis revealed a high heterogeneity among SSTR2 particles, both under basal and stimulated conditions. The results of the MSD analysis were also used to classify the SSTR2 trajectories into four groups corresponding to receptors that were either virtually immobile or were characterized by a confined, directed or Brownian motion (sub-, super-, normal diffusion, respectively) (Figure 2A

and C).

Prior to stimulation, the mobile fraction was 94.6%. Short-term stimulation with BIM23120 caused a statistically significant increase in the fraction of virtually immobile SSTR2s compared to basal conditions (16.5% vs. 5.4 %, respectively) and a corresponding reduction of around 3% for the remaining fractions (Figure 2C). This was accompanied by a general reduction of the average diffusion coefficient (*D*) values estimated for the three mobile fractions compared to basal conditions (from 0.062 to 0.077 $\mu m^2 \cdot s^{-1}$, from 0.099 to 0.114 $\mu m^2 \cdot s^{-1}$ and from 0.115 to 0.130 $\mu m^2 \cdot s^{-1}$ for sub-, normal and super-diffusion fractions, respectively) (Figure 2D).

To investigate the possible involvement of the cortical actin cytoskeleton in anchoring and/or limiting the mobility of SSTR2s (23, 26, 39), we simultaneously imaged actin fibers via co-transfection of LifeAct-GFP (29) (Figure 2E). We found that SSTR2s were preferentially localized along actin fibers, as indicated by positive colocalization index values (for details about the analysis see ref. 26). The preferential localization of SSTR2s along actin filaments was further enhanced by BIM23120 stimulation (Figure 2F). These data suggested that SSTR2s were either directly or indirectly interacting with the underlying actin cytoskeleton.

Filamin A controls SSTR2 mobility at the plasma membrane

The subcortical cytoskeleton has been shown to provide anchor points for receptors and other membrane proteins as well as barriers to their diffusion – a concept known as the fence-and-picket model (39), ultimately resulting in the formation of subdomains at the plasma membrane (26, 39). Since FLNA is a major actin binding protein and has been previously suggested to interact with SSTR2 based on *in vitro* results (17, 22), we investigated whether FLNA-SSTR2 interactions occur in living cells and play a role in SSTR2 spatial arrangement and mobility.

For this purpose, we co-expressed SNAP-SSTR2 and CLIP-FLNA in CHO cells at low

physiological levels and simultaneously imaged individual SSTR2 and FLNA molecules by fast two-color TIRF microscopy followed by automated single particle tracking. In a subset of experiments, we additionally labeled actin fibers via co-transfection of LifeAct-GFP. Importantly, we observed individual SSTR2s transiently stopping at sites on actin fibers where a FLNA molecule was also located (Figure 3A and Supplemental Fig. S3, Supplemental Movie 1 and Supplemental Movie 2). These results revealed that SSTR2 undergo transient interactions with FLNA lasting approximately 0.521 seconds, which resulted in a preferential localization of SSTR2s along actin fibers.

We then explored the overall contribution of SSTR2–FLNA interactions on SSTR2 mobility at the plasma membrane. In order to interfere with SSTR2–FLNA interactions, we co-expressed a FLNA fragment corresponding to domains 19 and 20 (FLNA 19-20), which has been previously suggested to exert a dominant negative effect on the binding of SSTR2 to endogenous FLNA (17). The FLNA fragment encompassing repeats 17 and 18 (FLNA 17-18) was used as control (17). Individual SSTR2 particles retained their heterogeneous diffusion dynamics, independently of the presence of the dominant negative fragment (FLNA 19-20), as shown by a MSD analysis (Figure 3B). However, the average diffusion coefficients measured with FLNA 19-20 under basal conditions were overall higher than with the control fragment (FLNA 17-18) and these differences reached statistical significance for the super-diffusing particles, suggesting that the previously observed dynamic SSTR2-FLNA interactions on acting fibers contributed to slowing down SSTR2 diffusion at the plasma membrane (Figure 3C).

Disrupting SSTR2–FLNA interactions hampers agonist-dependent SSTR2 clustering

Since interactions with the actin cytoskeleton have also been suggested to play a possible role in receptor clustering (40, 41), we simultaneously imaged SSTR2, FLNA and actin at later time

points. TIRF images acquired in CHO cells stimulated with BIM23120 for 10 min showed the formation of SSTR2 clusters, which were absent under basal conditions (Figure 4A, arrowheads). Interestingly, we found that these clusters had a tendency to be aligned along actin fibers and that FLNA was often present together with SSTR2 in these clusters. Similar results were also obtained in confocal microscopy experiments (Figure 4B), in which we used higher SSTR2 and FLNA expression levels to facilitate the detection of the clusters. Co-expression of the dominant negative FLNA fragment (FLNA 19-20) caused a statistically significant reduction of the colocalization of SSTR2 clusters with actin (Figure 4B and C). This was accompanied by a statistically significant reduction in the size of SSTR2 clusters (Figure 4D) and a tendency towards a reduction of their number (Figure 4E). These findings indicate a role of FLNA in the formation and correct spatial arrangement of SSTR2 clusters along actin fibers.

FLNA is required for efficient clathrin-mediated endocytosis of SSTR2

Like for many other GPCRs, prolonged SSTR2 stimulation leads to its internalization, mainly via clathrin-mediated endocytosis (CME) (42, 43). Since actin and FLNA have been implicated in CME (40, 44–49), we investigated whether FLNA played a role in SSTR2 internalization. For this purpose, we simultaneously imaged the adaptor protein complex 2 (AP-2), which participates in both clathrin coated pit (CCP) initiation and recruitment of receptors to nascent CCPs, and is a widely used marker of CME (28). Confocal microscopy showed that, in cells expressing the FLNA17-18 control fragment and stimulated with BIM23120 for 10 min, a relevant fraction of SSTR2 clusters contained AP-2 (Figure 5A, white spots). These structures containing SSTR2s in nascent CCPs were observed to a remarkably lesser extent in FLNA 19-20 expressing cells (Figure 5A). Indeed, Manders' coefficient analysis demonstrated that the degree of SSTR2 colocalization with AP-2-positive pits (MCC1) was significantly reduced (from 37.1 ± 8.7% to

18.9 ± 9.9%) in the presence of the dominant-negative FLNA19-20 fragment. This was accompanied by a similar reduction in the colocalization of AP2 with SSTR2 (MCC2; Figure 5B). These data suggested that whereas interfering with SSTR2–FLNA interactions had significant but modest effects on the formation of SSTR2 clusters – consistent with the results of Figure 4B – it largely impaired their coupling to CCPs and, thus, the recruitment of SSTR2 to CCPs.

Interfering with SSTR2–FLNA interactions impairs SSTR2 internalization

Given our observation that FLNA is required for SSTR2 recruitment to CCPs, we further studied the impact of FLNA–SSTR2 interactions on SSTR2 internalization. For this purpose, we analyzed the subcellular localization of SSTR2 by confocal microscopy in CHO cells transiently cotransfected with SNAP-SSTR2 and either FLNA17-18 or FLNA19-20 fragments and incubated with or without the agonist BIM23120 for up to 60 min. Under basal conditions, SSTR2 was virtually exclusively located at the plasma membrane, both in the presence of FLNA17-18 and FLNA19-20. As expected, BIM23120 induced a robust, time-dependent internalization and accumulation of SSTR2 in vesicles scattered throughout the cytoplasm in the presence of the control FLNA17-18 fragment (amount of internalized receptor of 54.8%, 68.7% and 71.4% after 15, 30 and 60 min, respectively, corresponding to a fR of 0.45, 0.31 and 0.27, respectively) (Figure 6A and B). In contrast, SSTR2 internalization was significantly impaired in the presence of the dominant negative FLNA19-20 fragment (amount of internalized receptor of 41.5%, 45.4% and 53% after 15, 30 and 60 min, respectively, corresponding to a fR of 0.58, 0.55 and 0.47, respectively) (Figure 6A and B).

An assay based on biotinylation of cell-surface receptors further showed that SSTR2 internalization was impaired in cells expressing the dominant negative FLNA19-20 fragment

compared to cells expressing the control FLNA17-18 fragment (39.1 ± 6.7% vs. 9.0 ± 2.9%, respectively; *, P<0.01 vs. FLNA 17-18 expressing cells) (Figure 6C).

4. Discussion

The present study investigated the spatiotemporal dynamics of SSTR2 at the plasma membrane, revealing a crucial active role of the cytoskeletal adaptor protein FLNA in coordinating SSTR2 diffusion dynamics and internalization. Our major findings suggest a model whereby FLNA molecules transiently interact with agonist-activated SSTR2s, facilitating their loose attachment to subcortical actin fibers and, thus, controlling their spatial arrangement and mobility. By controlling the localization of SSTR2s relative to the actin cytoskeleton, FLNA-SSTR2 interactions promote SSTR2 internalization via facilitating the coupling between receptor clustering and accumulation in CCPs, both processes that occur with intervention of the actin cytoskeleton (45–49) (Figure 7).

Our single-molecule data indicate that SSTR2 lateral diffusion is modulated by agonist stimulation. The very high percentage (94.6%) of the mobile fraction seen under basal conditions is in agreement with fluorescence recovery after photobleaching (FRAP) results obtained with murine SST2a in living hippocampal neurons (50). Interestingly, our data show a significant increase in the fraction of virtually immobile receptors and lower diffusion coefficients within the mobile fractions in stimulated CHO cells in comparison with the basal state. These findings indicate that only a minor fraction of SSTR2s is associated with the cytoskeleton in the resting state, whereas such cytoskeletal interactions occur more frequently when the receptors are activated (Figure 2). Few controversial data are present in the literature regarding the role of FLNA in regulating the diffusion of cell surface proteins (51, 52). Our MSD analysis shows that in the presence of FLNA19-20, used to interfere with SSTR2-FLNA interactions (17, 22),

SSTR2s are more mobile compared to control cells (Figure 3). Overall, our findings are in agreement with the fence-and-picket model of the plasma membrane (53, 54), according to which integral membrane proteins ("pickets") and barriers provided by the subcortical cytoskeleton ("fences") compartmentalize the plasma membrane into small domains where receptors are loosely trapped. Our recently published data indicate that this phenomenon contributes to the formation of hot spots where receptors preferentially accumulate and signal (26). The findings of the present study suggest the FLNA might act as a scaffold to preferentially recruit ligand-activated receptors at specific actin-rich regions of the plasma membrane, which, in turn, would facilitate SSTR2 recruitment in CCPs and their internalization.

Previous studies have implicated the actin cytoskeleton in the maintenance of discrete sites of CCP assembling on the plasma membrane (44–49). When we investigated SSTR2 dynamics at higher receptor expression levels (obtained after 48 h transfection) than the ones achieved in previous single molecule experiments (obtained after 4-18 h transfection), we observed receptor clustering upon prolonged stimulation. However, both the colocalization between SSTR2 clusters and actin filaments and the size of SSTR2 clusters were significantly reduced in the presence of FLNA19-20, the dominant negative fragment of FLNA (Figure 4). These findings suggest that FLNA acts by linking SSTR2 clusters, CCPs and subcortical actin fibers. A similar clathrin–actin linking role has been previously suggested for other actin binding proteins such as the huntingtin-interacting protein 1 related protein (Hip1R) (46). Among the different proteins that cooperate in the formation of CCPs, AP-2 is one of the key co-factors that promotes CCP initiation at the plasma membrane to then disengage from CCPs immediately before vesicle internalization (55). In particular, the association of membrane-bound AP-2 with cytosolic clathrin triskelions favors cargo protein capture by the activated μ2 subunit of AP-2 (28, 56). Intriguingly, our data indicate

that interfering with SSTR2-FLNA interactions reduces the colocalization between agonist-induced SSTR2 clusters and AP2-containing CCPs, further supporting our hypothesis of a role for FLNA in the spatial coordination of receptor clustering and recruitment into nascent CCPs (Figure 5).

It has been previously postulated that the actin cytoskeleton might also play a mechanical role in CME, providing the force to drive invagination and translocation of the nascent vesicles into the cytoplasm (57, 58). Our data suggest that interactions with FLNA are required to initiate and sustain the overall process of clathrin-dependent SSTR2 internalization (40, 41, 52, 59–64). Our imaging and biochemical data show that SSTR2 is rapidly and efficiently internalized in CHO cells (about 70% internalization after 30 min of agonist exposure), in agreement with previous observations (42, 65–67). However, SSTR2 internalization was strongly impaired when FLNA–SSTR2 association was inhibited (Figure 6). This is in accordance with our previous observation that FLNA–SSTR2 binding is not required for SSTR2 expression and membrane localization in GH-secreting tumor cells but is rather involved in SSTR2 signaling and downregulation (17).

In conclusion, our findings reveal that SSTR2–FLNA undergo transient interactions in living cells, which dynamically link SSTR2s to the actin cytoskeleton. These interactions with FLNA and actin fibers regulate SSTR2 spatial arrangement and mobility and are required for coupling agonist-dependent SSTR2 clustering to its recruitment to CCPs and, ultimately, its internalization. These results, together with our previous observation that FLNA is involved in the regulation of SSTR2 signaling and downregulation (17), indicate FLNA as a novel potential target to modulate the amount of active SSTR2s at the plasma membrane, with possible implications for the therapy of pharmacologically resistant GH-secreting pituitary tumors.

7. Acknowledgments

We thank S. Schulz (Institute of Pharmacology and Toxicology, Jena University Hospital, Friedrich Schiller University Jena, Drackendorfer Str. 1, 07747, Jena, Germany), A.M. Aragay (Molecular Biology Institute of Barcelona, Spanish National Research Council (CSIC), 08028 Barcelona, Spain) and T. Kirchhausen and E. Cocucci (Department of Pediatrics, Harvard Medical School, Boston, MA 02115, USA) for the plasmids expressing human wild-type SSTR2, eGFP-FLNA and eGFP-AP-2, respectively. **Author contributions**. D.T. designed, performed, analyzed the experiments and wrote the manuscript; M.-L.J. performed, analyzed the experiments and wrote the manuscript; E.P. designed the experiments and critically reviewed the manuscript; E.G., T.S. and U.Z. contributed to the experiments; A.S. provided intellectual input; G.M. and D.C. supervised the project, provided intellectual input and critically reviewed the manuscript. **Fundings.** This study was supported by Associazione Italiana Ricerca sul Cancro (grants IG 2014-15507 and IG 2017-20594 to G.M.), Pfizer grants (WI207277 to G.M. and WI219094 to E.P.), Ricerca Corrente Funds from the Italian Ministry of Health, Progetti di Ricerca di Interesse Nazionale (grant 2015ZHKFTA to G.M.), the Deutsche Forschungsgemeinschaft (grant CA 1014/1-1 to D.C.) and Sonderforschungsbereich/Transregio (166–Project C1 to D.C.).

8. References

1. Bruns C, Weckbecker G, Raulf F, Kaupmann K, Schoeffter P, Hoyer D, Lübbert H. Molecular pharmacology of somatostatin-receptor subtypes. *Ann NY Acad Sci.* 1994;733:138–146.

2. Patel YC. Somatostatin and its receptor family. *Front Neuroendocrinol.* 1999;20:157–198.

3. Buscail L, Estève JP, Saint-Laurent N, Bertrand V, Reisine T, O'Carroll AM, Bell GI, Schally AV, Vaysse N, Susini C. Inhibition of cell proliferation by the somatostatin analogue RC-160 is mediated by somatostatin receptor subtypes SSTR2 and SSTR5 through different mechanisms. *Proc. Natl. Acad. Sci. USA.* 1995;92:1580–1584.

4. Cordelier P, Estève JP, Bousquet C, Delesque N, O'Carroll AM, Schally AV, Vaysse N, Susini C, Buscail L. Characterization of the antiproliferative signal mediated by the somatostatin receptor subtype sst5. *Proc Natl Acad Sci USA.* 1997;94:9343–9348.

5. Lopez F, Esteve JP, Buscali L, Delesqu N, Saint-Laurent N, Theveniau M, Nahmias C, Vaysse N, Susini C. The tyrosine phosphatase SHP-1 associates with the sst2 somatostatin receptor and is an essential component of sst2-mediated inhibitory growth signaling. *J Biol Chem* 1997;272:24448–24454.

6. Ben-Shlomo A, Melmed S. Pituitary somatostatin receptor signaling. *Trends Endocrinol Metab.* 2010;21:123–133.

7. Nielsen S, Mellemkjaer S, Rasmussen LM, Ledet T, Olsen N, Bojsen-Møller M, Astrup J, Weeke J, Jørgensen JO. Expression of somatostatin receptors on human pituitary adenomas in vivo and ex vivo. *J Endocrinol Invest.* 2001;24:430–437.

8. Taboada GF, Luque RM, Bastos W, Guimarães RF, Marcondes JB, Chimelli LM, Fontes R, Mata PJ, Filho PN, Carvalho DP, Kineman RD, Gadelha MR. Quantitative analysis of somatostatin receptor subtype (SSTR1-5) gene expression levels in somatotropinomas and non-functioning pituitary adenomas. *Eur J Endocrinol.* 2007;156:65–74.

9. Ben-Shlomo A, Melmed S. Acromegaly. *Endocrinol Metab Clin North Am.* 2008;37:101–122.

10. Melmed S, Colao A, Barkan A, Molitch M, Grossman AB, Kleinberg D, Clemmons D, Chanson P, Laws E, Schlechte J, Vance ML, Ho K, Giustina A. Guidelines for acromegaly management: an update. *J Clin Endocrinol Metab.* 2009;94:1509–1517.

11. Fleseriu M. The role of combination medical therapy in acromegaly: hope for the nonresponsive patient. *Curr Opin Endocrinol Diabetes Obes.* 2013;20:321–329.

12. Casarini AP, Pinto EM, Jallad RS, Giorgi RR, Giannella-Neto D, Bronstein MD. Dissociation between tumor shrinkage and hormonal response during somatostatin analog treatment in an acromegalic patient: preferential expression of somatostatin receptor subtype 3. *J. Endocrinol Invest.* 2006;29:826–830.

13. Resmini E, Dadati P, Ravetti JL, Zona G, Spaziante R, Saveanu A, Jaquet P, Culler MD, Bianchi F, Rebora A, Minuto F, Ferone D. Rapid pituitary tumor shrinkage with dissociation between antiproliferative and antisecretory effects of a long-acting octreotide in an acromegalic patient. *J Clin Endocrinol Metab.* 2007;92:1592–1599.

14. Fougner SL, Bollerslev J, Latif F, Hald JK, Lund T, Ramm-Pettersen J, Berg JP. Low levels of raf kinase inhibitory protein in growth hormone-secreting pituitary adenomas correlate with poor response to octreotide treatment. *J Clin Endocrinol Metab.* 2008;93:1211–1216.

15. Tuominen I, Heliövaara E, Raitila A, Rautiainen MR, Mehine M, Katainen R, Donner I, Aittomäki V, Lehtonen HJ, Ahlsten M, Kivipelto L, Schalin-Jäntti C, Arola J, Hautaniemi S, Karhu A. AIP inactivation leads to pituitary tumorigenesis through defective Gαi-cAMP signaling. *Oncogene.* 2015;34:1174–1184.

16. Gatto F, Feelders R, van der Pas R, Kros JM, Dogan F, van Koetsveld PM, van der Lelij AJ, Neggers SJ, Minuto F, de Herder W, Lamberts SW, Ferone D, Hofland LJ. β-Arrestin 1 and 2 and G protein-coupled receptor kinase 2 expression in pituitary adenomas: role in the regulation of response to somatostatin analogue treatment in patients with acromegaly. *Endocrinology.* 2013;154:4715–4725.

17. Peverelli E, Giardino E, Treppiedi D, Vitali E, Cambiaghi V, Locatelli M, Lasio GB, Spada A, Lania AG, Mantovani G. Filamin A (FLNA) plays an essential role in somatostatin receptor 2 (SST2) signaling and stabilization after agonist stimulation in human and rat somatotroph tumor cells. *Endocrinology.* 2014;155:2932–2941.

18. Gatto F, Biermasz NR, Feelders RA, Kros JM, Dogan F, van der Lely AJ, Neggers SJ, Lamberts SW, Pereira AM, Ferone D, Hofland LJ. Low beta-arrestin expression correlates with the responsiveness to long-term somatostatin analog treatment in acromegaly. *Eur J Endocrinol.* 2016;174:651–62.

19. Treppiedi D, Peverelli E, Giardino E, Ferrante E, Calebiro D, Spada A, Mantovani G. Somatostatin Receptor Type 2 (SSTR2) Internalization and Intracellular Trafficking in Pituitary GH-Secreting Adenomas: Role of Scaffold Proteins and Implications for Pharmacological Resistance. *Horm Metab Res.* 2016;49:259–268.

20. Stossel TP, Condeelis J, Cooley L, Hartwig JH, Noegel A, Schleicher M, Shapiro SS. Filamins as integrators of cell mechanics and signalling. *Nat Rev Mol Cell Biol.* 2001;2:138–145.

21. Nakamura F, Stossel TP, Hartwig JH. The filamins: organizers of cell structure and function. *Cell Adh Migr.* 2011;5:160–169.

22. Najib S, Saint-Laurent N, Estève JP, Schulz S, Boutet-Robinet E, Fourmy D, Lättig J, Mollereau C, Pyronnet S, Susini C, Bousquet C. A switch of G protein-coupled receptor binding preference from phosphoinositide 3-kinase (PI3K)-p85 to filamin A negatively controls the PI3K pathway. *Mol Cell Biol.* 2012;32:1004–1016.

23. Calebiro D, Rieken F, Wagner J, Sungkaworn T, Zabel U, Borzi A, Cocucci E, Zürn A, Lohse MJ. Single-molecule analysis of fluorescently labeled G-protein-coupled receptors reveals complexes with distinct dynamics and organization. *Proc Natl Acad Sci. USA.* 2013;110:743–748.

24. Sungkaworn T, Rieken F, Lohse MJ, Calebiro D. High-resolution spatiotemporal analysis of receptor dynamics by single-molecule fluorescence microscopy. *J Vis Exp.* 2014;89:e51784.

25. Calebiro D, Sungkaworn T. Single-Molecule Imaging of GPCR Interactions. *Trends Pharmacol Sci*. 2017;39:109–122.

26. Sungkaworn T, Jobin ML, Burnecki K, Weron A, Lohse MJ, Calebiro D. Single-molecule imaging reveals receptor-G protein interactions at cell surface hot spots. *Nature.* 2017;550:543–547.

27. Planagumà J, Minsaas L, Pons M, Myhren L, Garrido G, Aragay AM. Filamin A-hinge region 1-EGFP: a novel tool for tracking the cellular functions of filamin A in real-time. PLoS One. 2012;7:e40864.

28. Cocucci E, Aguet F, Boulant S, Kirchhausen T. The first five seconds in the life of a clathrin-coated pit. *Cell.* 2012;150:495–507.

29. Riedl J, Crevenna AH, Kessenbrock K, Yu JH, Neukirchen D, Bista M, Bradke F, Jenne D, Holak TA, Werb Z, Sixt M, Wedlich-Soldner R. Lifeact: a versatile marker to visualize F-actin. *Nat Methods.* 2008;5:605–607.

30. Nikolaev VO, Bünemann M, Hein L, Hannawacker A, Lohse MJ. Novel single chain cAMP sensors for receptor-induced signal propagation. *J Biol Chem.* 2004;279:37215–37218.

31. Calebiro D, Nikolaev VO, Gagliani MC, de Filippis T, Dees C, Tacchetti C, Persani L, Lohse MJ. Persistent cAMP-signals triggered by internalized G-protein-coupled receptors. *PLoS Biol.* 2009;7:e1000172.

32. Godbole A, Lyga S, Lohse MJ, Calebiro D. Internalized TSH receptors en route to the TGN induce local Gs-protein signaling and gene transcription. *Nat Commun.* 2017;8:443.

33. Jaqaman K, Loerke D, Mettlen M, Kuwata H, Grinstein S, Schmid SL, Danuser G. Robust single-particle tracking in live-cell time-lapse sequences. *Nat Methods.* 2008;5:695–702.

34. Ibach J, Radon Y, Gelléri M, Sonntag MH, Brunsveld L, Bastiaens PI, Verveer PJ. Single Particle Tracking Reveals that EGFR Signaling Activity Is Amplified in Clathrin-Coated Pits. *PLoS One.* 2015;10:e0143162.

35. Manders EMM, Verbeek FJ, Aten JA. Measurement of colocalization of objects in dual-color confocal images. *J Microsc.* 1993;169:375–382.

36. Peverelli E, Mantovani G, Calebiro D, Doni A, Bondioni S, Lania A, Beck-Peccoz P, Spada A. The third intracellular loop of the human somatostatin receptor 5 is crucial for arrestin binding and receptor internalization after somatostatin stimulation. *Mol Endocrinol.* 2008;**22**:676–688.

552 37. Keppler A, Gendreizig S, Gronemeyer T, Pick H, Vogel H, Johnsson K. A general method
553 for the covalent labeling of fusion proteins with small molecules in vivo. *Nat Biotechnol*
554 2003;21:86–89.

555 38. Gautier A, Juillerat A, Heinis C, Corrêa Jr IR, Kindermann M, Beaufils F, Johnsson K. An
556 engineered protein tag for multiprotein labeling in living cells. *Chem Biol.* 2008;15:128–136.

557 39. Kusumi A, Sako Y, Yamamoto M. Confined lateral diffusion of membrane receptors as
558 studied by single particle tracking (nanovid microscopy). Effects of calcium-induced
559 differentiation in cultured epithelial cells. *Biophys J.* 1993;65:2021–2040.

560 40. Minsaas L, Planagumà J, Madziva M, Krakstad BF, Masià-Balagué M, Katz AA, Aragay
561 AM., Filamin a binds to CCR2B and regulates its internalization. *PLoS One.* 2010;5:e12212.

562 41. Noam Y, Ehrengruber MU, Koh A, Feyen P, Manders EM, Abbott GW, Wadman WJ, Baram
563 TZ. Filamin A promotes dynamin-dependent internalization of hyperpolarization-activated cyclic
564 nucleotide-gated type 1 (HCN1) channels and restricts Ih in hippocampal neurons. *J Biol Chem.*
565 2014;289:5889–5903.

566 42. Koenig JA, Edwardson JM, Humphrey PP. Somatostatin receptors in Neuro2A
567 neuroblastoma cells: ligand internalization. *Br J Pharmacol.* 1997;120:52–59.

568 43. Pierce KL, Lefkowitz RJ. Classical and new roles of beta-arrestins in the regulation of G-
569 protein-coupled receptors. *Nat Rev Neurosci.* 2001;2:727–733.

570 44. Gaidarov I, Santini F, Warren RA, Keen JH. Spatial control of coated-pit dynamics in living
571 cells. *Nat Cell Biol.* 1999;1:1–7.

45.Qualmann B, Kessels MM, Kelly RB. Molecular links between endocytosis and the actin cytoskeleton. *J Cell Biol.* 2000;150:F111–116.

46. Bennett EM, Chen CY, Engqvist-Goldstein AE, Drubin DG, Brodsky FM. Clathrin hub expression dissociates the actin-binding protein Hip1R from coated pits and disrupts their alignment with the actin cytoskeleton. *Traffic.* 2001;2:851–858.

47. Merrifield CJ, Feldman ME, Wan L, Almers W. Imaging actin and dynamin recruitment during invagination of single clathrin-coated pits. *Nat Cell Biol.* 2002;4:691–698.

48. Qualmann B, Kessels MM. Endocytosis and the cytoskeleton. *Int Rev Cytol.* 2002;220:93–144.

49. Engqvist-Goldstein AE, Drubin DG. Actin assembly and endocytosis: from yeast to mammals. *Annu. Rev. Cell Dev Biol.* 2003;19:287–332.

50. Lelouvier B, Tamagno G, Kaindl AM, Roland A, Lelievre V, Le Verche V, Loudes C, Gressens P, Faivre-Baumann A, Lenkei Z, Dournaud P. Dynamics of somatostatin type 2A receptor cargoes in living hippocampal neurons. *J Neurosci.* 2008;28:4336–4349.

51. Sverdlov M, Shinin V, Place AT, Castellon M, Minshall RD. Filamin A regulates caveolae internalization and trafficking in endothelial cells. *Mol Biol Cell.* 2009;20:4531–4540.

52. Muriel O, Echarri A, Hellriegel C, Pavón DM, Beccari L, Del Pozo MA. Phosphorylated filamin A regulates actin-linked caveolae dynamics. *J Cell Sci.* 2011;124:2763–2776.

590 53. Tsuji A, Kawasaki K, Ohnishi S, Merkle H, Kusumi A. Regulation of band 3 mobilities in
591 erythrocyte ghost membranes by protein association and cytoskeletal meshwork. *Biochemistry.*
592 1988;27:7447–7452.

593 54. Kusumi A, Ike H, Nakada C, Murase K, Fujiwara T. Single-molecule tracking of membrane
594 molecules: plasma membrane compartmentalization and dynamic assembly of raft-philic
595 signaling molecules. *Semin Immunol.* 2005;17:3–21.

596 55. Rappoport JZ, Kemal S, Benmerah A, Simon SM. Dynamics of clathrin and adaptor proteins
597 during endocytosis. *Am J Physiol. Cell Physiol.* 2006;291:C1072–1081.

598 56. Rapoport I, Miyazaki M, Boll W, Duckworth B, Cantley LC, Shoelson S, Kirchhausen T.
599 Regulatory interactions in the recognition of endocytic sorting signals by AP-2 complexes.
600 *EMBO J.* 1997;16:2240–2250.

601 57. Giardini PA, Fletcher DA, Theriot JA. Compression forces generated by actin comet tails on
602 lipid vesicles. *Proc Natl Acad Sci U S A.* 2003;100:6493–6498.

603 58. Merrifield CJ, Qualmann B, Kessels MM, Almers W. Neural Wiskott Aldrich Syndrome
604 Protein (N-WASP) and the Arp2/3 complex are recruited to sites of clathrin-mediated
605 endocytosis in cultured fibroblasts. *Eur J Cell Biol.* 2004;83:13–18.

606 59. Koenig JA, Kaur R, Dodgeon I, Edwardson JM, Humphrey PP. Fates of endocytosed
607 somatostatin sst2 receptors and associated agonists. *Biochem J.* 1998;336:291–298.

608 60. Lin R, Karpa K, Kabbani N, Goldman-Rakic P, Levenson R. Dopamine D2 and D3 receptors
609 are linked to the actin cytoskeleton via interaction with filamin A. *Proc Natl Acad Sci. USA.*
610 2001;98:5258–5263.

611 61. Onoprishvili I, Andria ML, Kramer HK, Ancevska-Taneva N, Hiller JM, Simon EJ.
612 Interaction between the mu opioid receptor and filamin A is involved in receptor regulation and
613 trafficking. *Mol Pharmacol.* 2003;64:1092–1100.

614 62. Seck T, Baron R, Horne WC. Binding of filamin to the C-terminal tail of the calcitonin
615 receptor controls recycling. *J Biol Chem.* 2003;278:10408–10416.

616 63. Zhang M, Breitwieser GE. High affinity interaction with filamin A protects against calcium-
617 sensing receptor degradation. *J Biol Chem.* 2005;280:11140–11146.

618 64. Cho EY, Cho DI, Park JH, Kurose H, Caron MG, Kim KM. Roles of protein kinase C and
619 actin-binding protein 280 in the regulation of intracellular trafficking of dopamine D3 receptor.
620 *Mol Endocrinol.* 2007;21:2242–2254.

621 65. Liu Q, Cescato R, Dewi DA, Rivier J, Reubi JC, Schonbrunn A. Receptor signaling and
622 endocytosis are differentially regulated by somatostatin analogs. *Mol Pharmacol.* 2005;68:90–
623 101.

624 66. Liu Q, Dewi DA, Liu W, Bee MS, Schonbrunn A. Distinct phosphorylation sites in the
625 SST2A somatostatin receptor control internalization, desensitization, and arrestin binding. *Mol*
626 *Pharmacol.* 2008;73:292–304.

627 67. Cambiaghi V, Vitali E, Morone D, Peverelli E, Spada A, Mantovani G, Lania AG.
628 Identification of human somatostatin receptor 2 domains involved in internalization and signaling
629 in QGP-1 pancreatic neuroendocrine tumor cell line. *Endocrine.* 2017;56:146–157.

Figure 1.

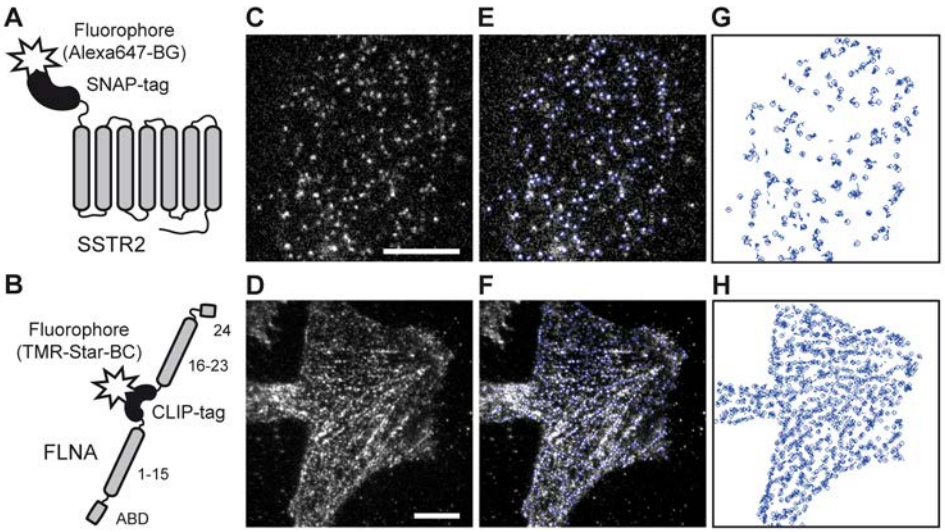

Figure 1. Single-molecule visualization and tracking of individual SSTR2 and FLNA particles at the plasma membrane of living cells.

(A and B) Schematic representation of the SNAP-SSTR2 (A) and CLIP-FLNA (B) constructs used in this study. (C-H) Single-molecule imaging. CHO cells were transfected with SNAP-SSTR2 (C) or CLIP-FLNA (D), labeled with Alexa647-BG or TMR-Star-BC substrates, respectively, and imaged by TIRF microscopy. Shown are single frames of representative image sequences (C and D), the same with overlaid in blue the individual trajectories obtained with the automated tracking algorithm (E and F) and the trajectories alone (G and H). The current position of each particle is indicated by a blue circle. Scale bars, 10 μm.

Figure 2.

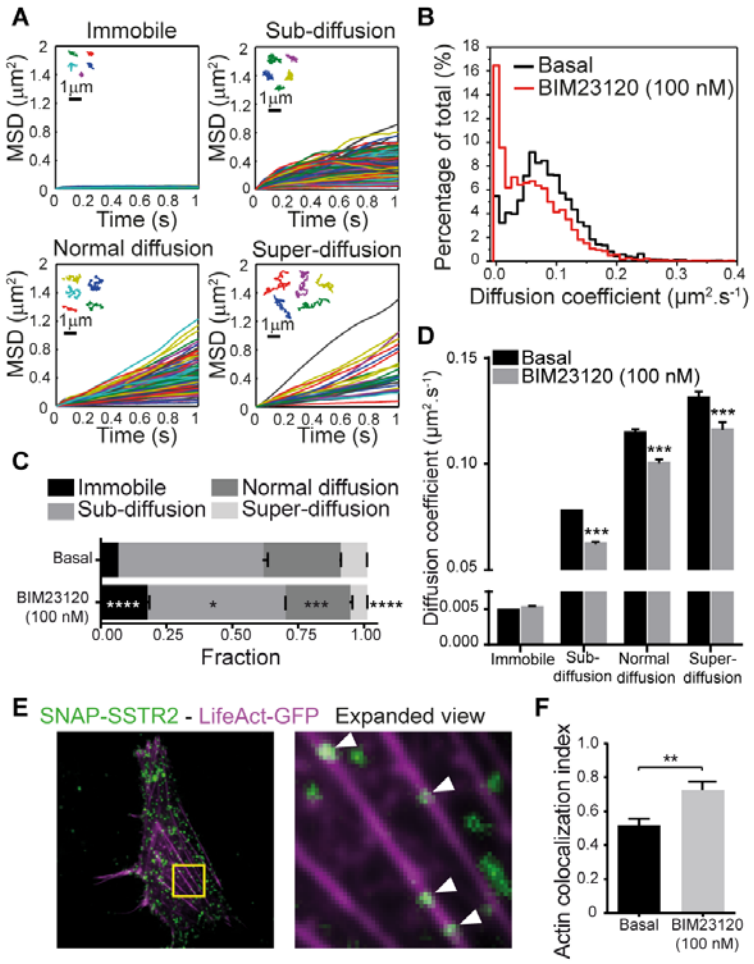

642

643 **Figure 2. SSTR2 diffusion dynamics at the plasma membrane is modified by agonist**
644 **stimulation.**

645 (A) MSD plots of representative SSTR2 trajectories classified into four groups based on their
646 mobility. (B) Diffusion coefficient distribution of SSTR2 particles calculated from the MSD
647 analysis and reported as percentage of total number of particles under basal (black) or stimulated
648 condition (red). (C) Frequency distributions of the trajectories in the four groups under basal and
649 stimulated conditions. (D) Average diffusion coefficients of each group shown in (C). Differences
650 in C and D are statistically significant by two-way ANOVA. *, P<0.05, ***, P<0.001 and ****,
651 P<0.0001 vs. corresponding basal condition by Tukey's multiple comparison test. (E)

Representative frame from a TIRF image sequence of SSTR2 particles (green) and actin fibers (magenta) in basal condition (left) and expanded view of the region marked with the yellow box (right). Arrowheads, individual SSTR2s localized along actin fibers. (F) Quantification of SSTR2 colocalization with actin fibers under basal and stimulated conditions. **, P<0.01 vs. basal condition by unpaired t-test. All data are mean ± SEM of three independent experiments.

Figure 3.

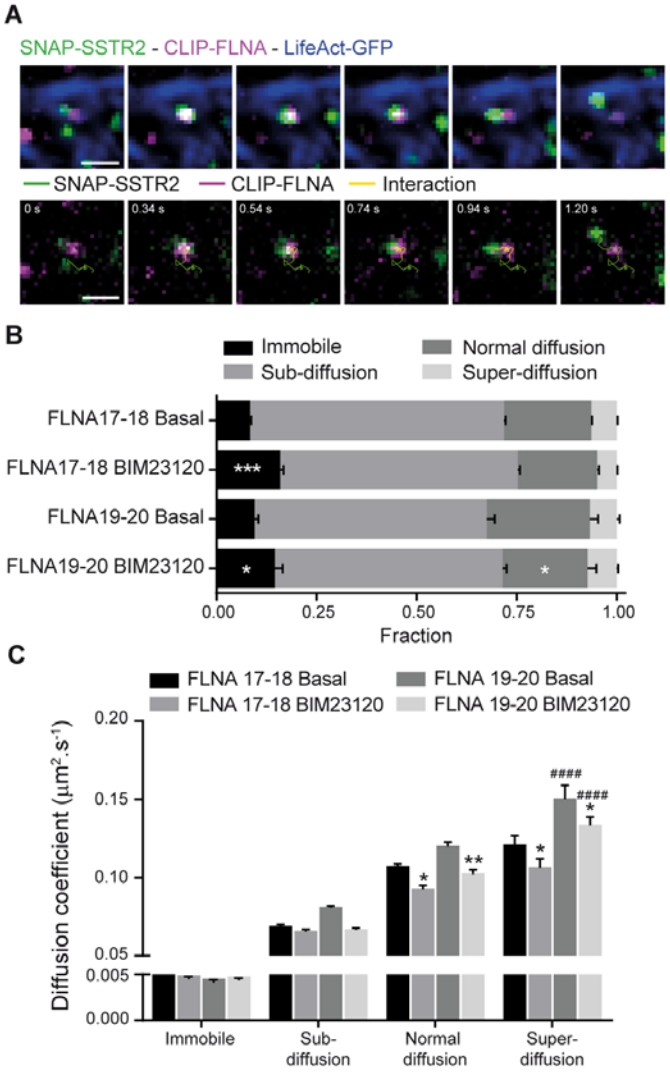

Figure 3. SSTR2 interactions with FLNA and actin at the plasma membrane regulate SSTR2 mobility.

(A) Top, selected frames from a representative TIRF image sequence acquired in CHO cells co-expressing SNAP-SSTR2 (green), CLIP-FLNA (magenta) and LifeAct-GFP (blue). Bottom, corresponding trajectories showing an example of a SSTR2 transiently colocalizing with a FLNA molecule on an actin fiber (yellow). Scale bars, 1 μm. (B) Frequency distributions of the trajectories classified in the four mobility groups in the presence of FLNA17-18 or FLNA19-20 fragments under both basal and stimulated conditions. (C) Average diffusion coefficients (*D*) corresponding to each group shown in (B). Differences in (B) and (C) are statistically significant by two-way ANOVA. *, $P<0.05$, **, $P<0.01$ and ***, $P<0.001$ by Tukey's multiple comparison test vs. basal condition; ####, $P<0.0001$ by Tukey's multiple comparison test vs. the corresponding fraction in the control (FLNA17-18). All data are mean ± SEM from three independent experiments.

Figure 4.

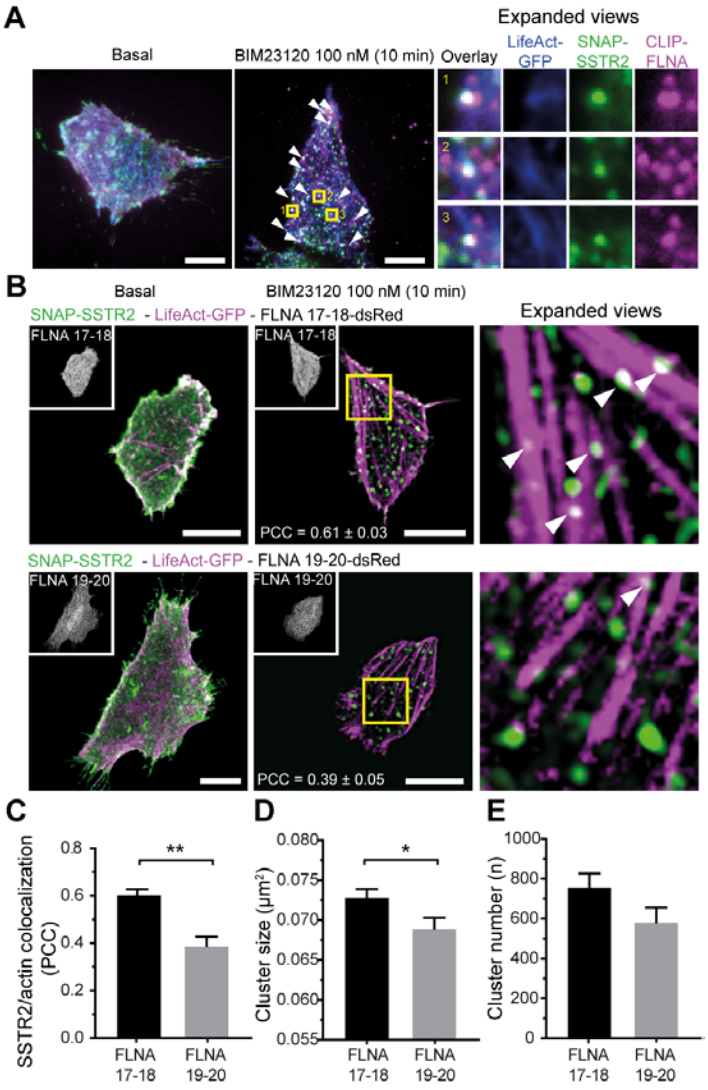

673

674 **Figure 4. Role of FLNA in agonist-dependent SSTR2 clustering.**

675 (A) Preferential alignment of SSTR2 clusters containing FLNA along actin fibers. CHO cells
676 were transfected to express LifeAct-GFP (blue) together with single-molecule levels of SNAP-
677 SSTR2 (green) and CLIP-FLNA (magenta). Shown are representative average intensity
678 projections of TIRF images sequences from three independent experiments under basal
679 conditions (left) or after stimulation with BIM23120 for 10 min (middle). Arrowheads, SSTR2
680 clusters containing FLNA aligned along actin fibers. Three examples of clusters are shown in
681 expanded views (right). Scale bars, 10 µm. (B) Effect of disrupting SSTR2–FLNA interactions on

682 the localization of SSTR2s along actin fibers. Shown are representative confocal optical sections
683 showing the plasma membrane of CHO cells cotransfected with LifeAct-GFP (magenta), SNAP-
684 SSTR2 (green) and FLNA17-18 or FLNA19-20 fragments under basal or stimulated conditions.
685 Insets, images showing high expression of the FLNA fragments. Arrowheads, SSTR2 clusters
686 aligned along actin fibers. Scale bars, 10 μm. (C-E) Quantitative analyses of images like those
687 shown in B. Reported are the Pearson's correlation coefficient (PCC) between SNAP-SSTR2 and
688 LifeAct-GFP images (C) as well as the number (D) and size (E) of SSTR2 clusters.**, $P < 0.01$
689 and *, $P < 0.05$ vs. FLNA 17-18 transfected cells by unpaired Student's *t* test. Data are mean ±
690 SEM of 15 cells from three independent experiments.

691 **Figure 5.**

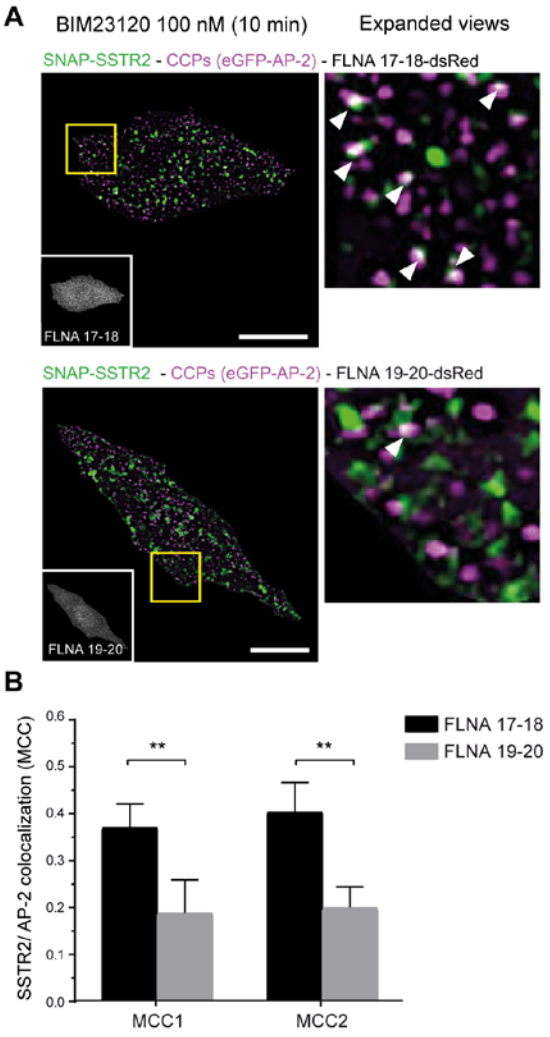

Figure 5. FLNA is required for efficient SSTR2 recruitment to CCPs.

(A) Effect of interfering with SSTR2–FLNA interactions on agonist-induced SSTR2 recruitment to CCPs. CHO cells were transiently cotransfected with SNAP-SSTR2 (green) and either FLNA 17-18 or FLNA 19-20 (insets) and immunostained for AP-2 (magenta). Shown are representative confocal images acquired at the level of the plasma membrane (left) and expanded views of the regions marked with the yellow boxes (right). Arrowheads, SSTR2 clusters colocalizing with AP-2 (white). Scale bars, 10 μm. (B) Quantitative analysis of images like those shown in A. The extent of pixel colocalization between SSTR2 and AP-2 is expressed as mean ± SEM of Manders' colocalization coefficients (MCC) where MCC1 represents the fraction of SSTR2 overlapping

with AP-2 and MCC2 the fraction of AP-2 overlapping with SSTR2 (Menders et al., 1993). For each condition, 15 cells from three independent experiments were analyzed. **, P<0.01 vs. FLNA 17-18 expressing cells by unpaired Student's *t* test.

Figure 6.

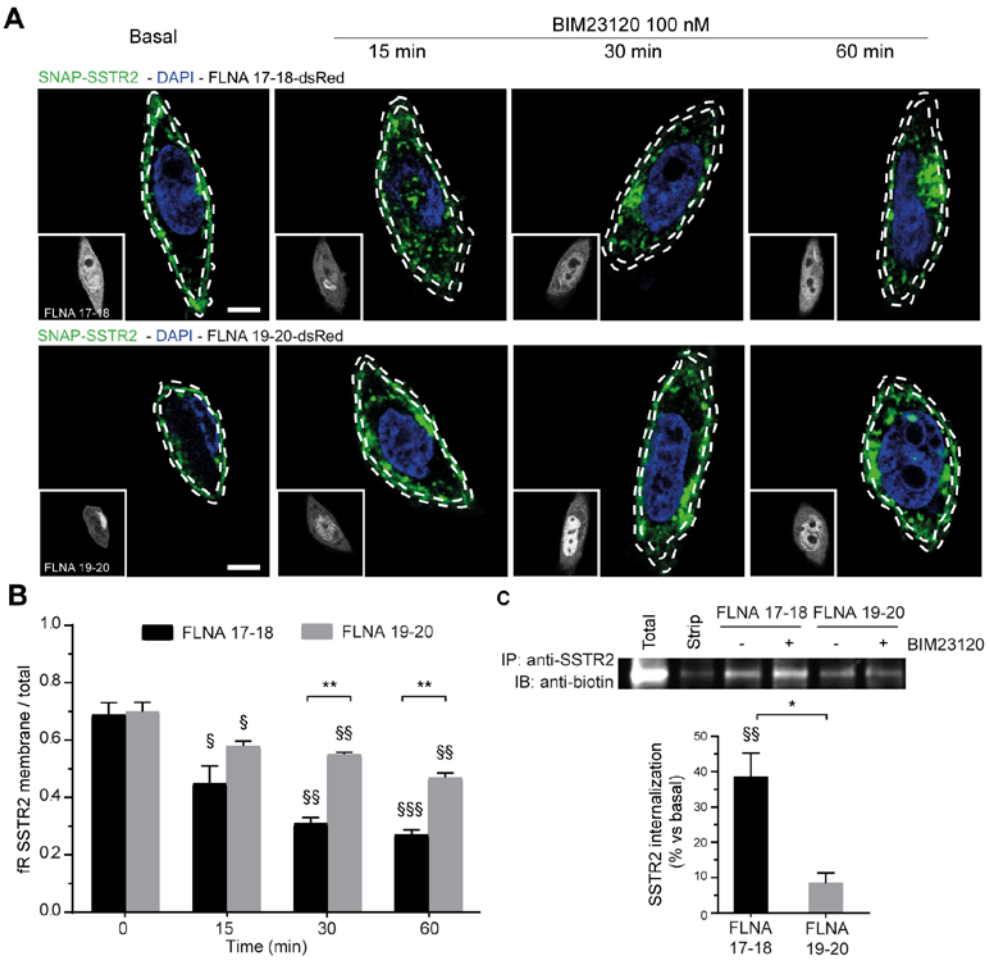

Figure 6. Inhibition of FLNA-SSTR2 interactions affects agonist-mediated SSTR2 internalization.

(A) CHO cells coexpressing SNAP-SSTR2 (green) and either FLNA17-18 (top) or FLNA19-20 (bottom) were incubated with 100 nM BIM23120 for 15, 30, and 60 min. Shown are representative confocal images acquired at the level of the nucleus. Hatched white lines represent the membrane area. Insets show the corresponding FLNA17-18 (top) or FLNA19-20 (bottom)

images. DAPI (blue) was used to stain the nucleus. Scale bars, 5 μm. (B) Quantitative analysis of SSTR2 internalization based on confocal images like those in A. For each group, at least 30 cells from three independent experiments were analyzed. Data are mean ± SEM *, P<0.05 and **, P<0.01 vs. FLNA 17-18 expressing cells; §, P<0.05, §§, P<0.01, §§§, P<0.001 vs. respective basal condition by unpaired Student's *t* test. (C) Quantification of SSTR2 internalization based on biotinylation of membrane receptors. CHO cells transiently cotransfected with FLNA 17-18 or FLNA 19-20 and wild-type SSTR2 were incubated with or without 100 nM BIM23120 for 30 min. SSTR2 was immunoprecipitated with a specific antibody and the internalized biotinylated SSTR2 was detected with an antibody recognizing biotin. Shown are the mean ± SEM of three independent experiments. *, P<0.05 vs. FLNA17-18 transfected cells; §§, P<0.01 vs. corresponding basal condition by unpaired Student's *t* test.

Figure 7.

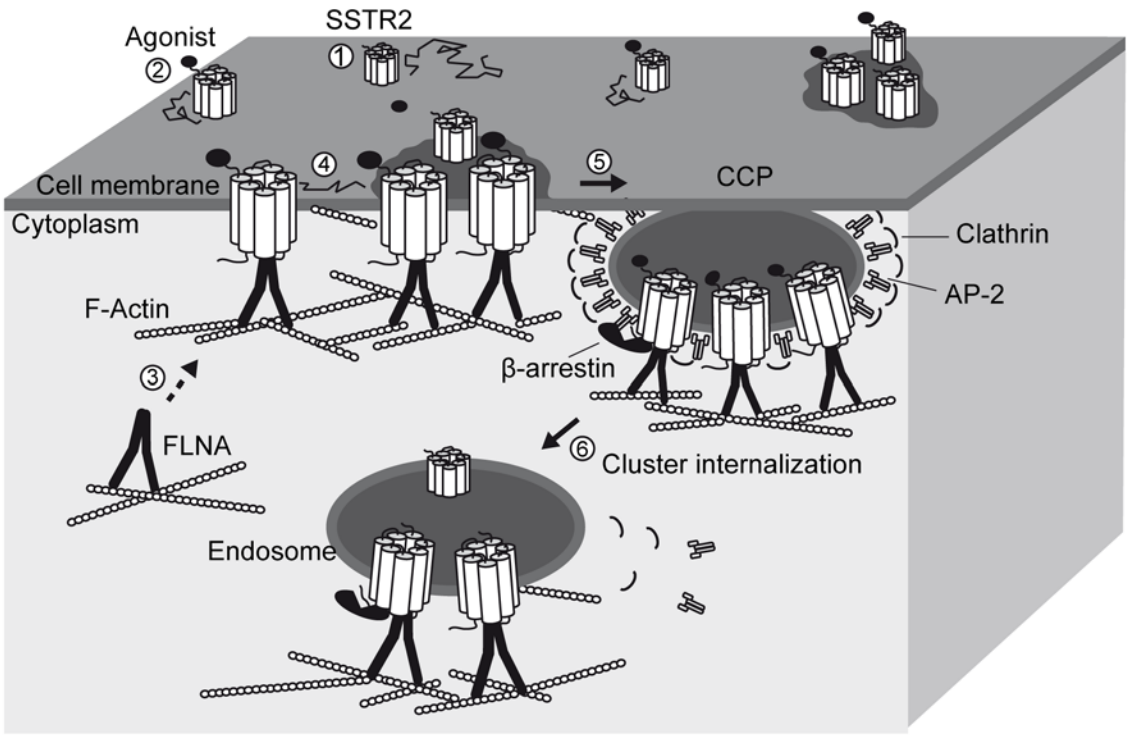

Figure 7. Proposed model for FLNA role in SSTR2 diffusion dynamics and internalization.

Under resting conditions, SSTR2s diffuse at the cell surface (1). Agonist binding (2) promotes FLNA recruitment to SSTR2s (3), which increases their interaction with actin fibers. This favors the formation of SSTR2 clusters and their correct localization in actin-rich regions of the plasma membrane (4). These events promote the recruitment of SSTR2s to CCPs (5) and, ultimately, their internalization (6).

Supplementary Data

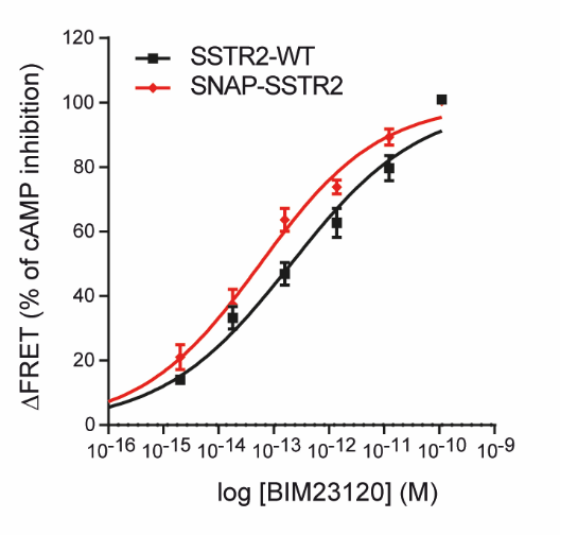

Supplemental Figure 1.

Functional characterization of SNAP-SSTR2 construct. HEK293A cells were co-transfected with SNAP-SSTR2 or wild-type SSTR2 and the FRET sensor for cAMP Epac1-camps. Cells were prestimulated with forskolin to activate adenylyl cyclases followed by incubation with increasing concentrations of the SSTR2-selective agonist BIM23120. The resulting inhibition of cAMP production was measured in real time by FRET microscopy. The SNAP-SSTR2 construct is fully functional, as shown by cAMP concentration-response dependencies comparable to those

observed with wild-type SSTR2. Data are mean ± SEM of 10 cells from three independent experiments.

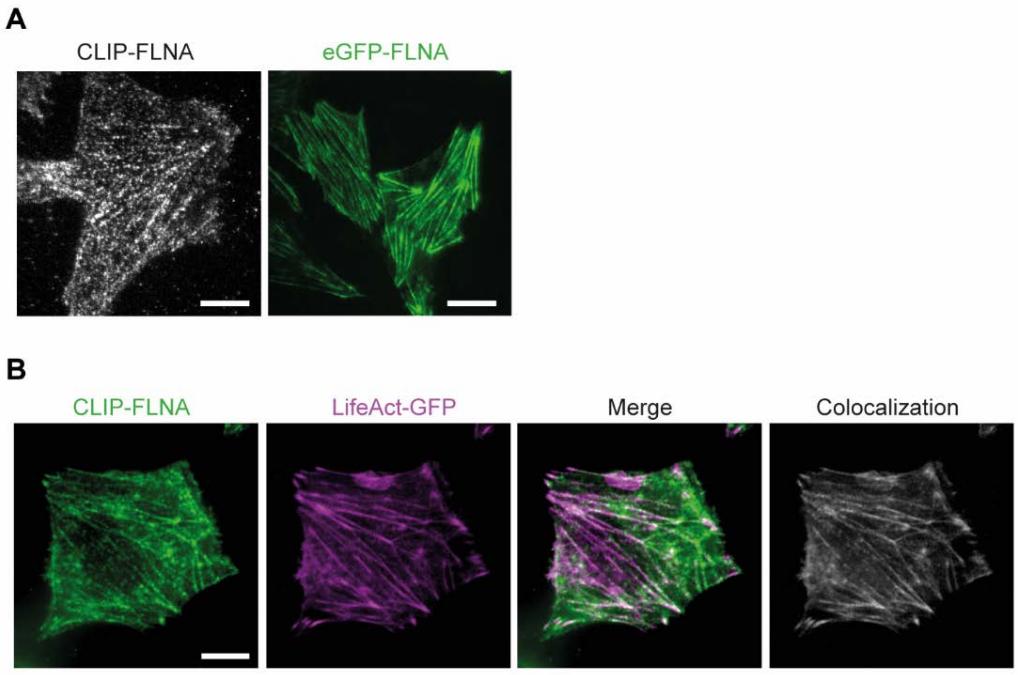

Supplemental Figure 2.

Validation of CLIP-FLNA construct. (A) TIRF images of CHO cells transfected with CLIP-FLNA or eGFP-FLNA, respectively. The CLIP-FLNA construct displays a normal arrangement along stress fibers, similar to what observed with eGFP-FLNA. (B) TIRF images of CHO cell cotransfected with CLIP-FLNA (green) and LifeAct-GFP (magenta). The resulting merge image is shown. Colocalization between CLIP-FLNA and actin filaments was analyzed by NIH ImageJ software and is shown in white, confirming the actin-binding property of the CLIP-FLNA construct. Scale bars, 10 µm.

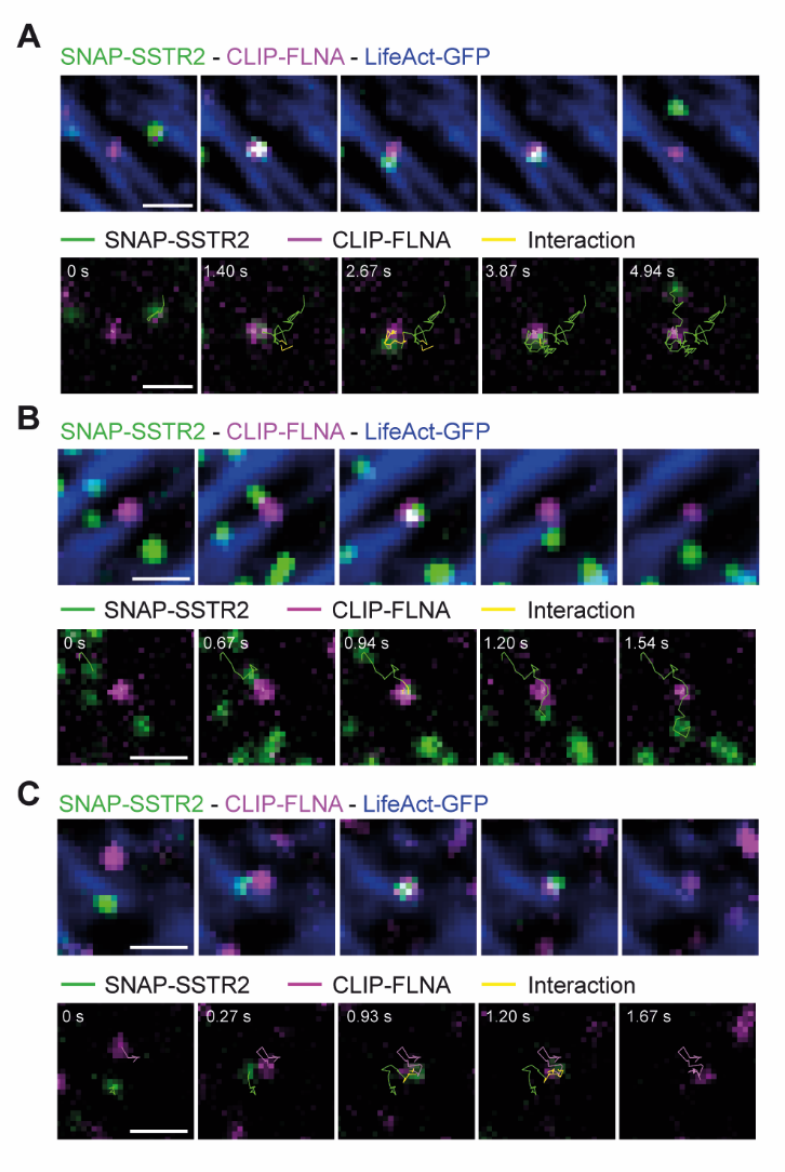

Supplemental Figure 3.

Single-molecule visualization of SSTR2 colocalizing with FLNA and actin at the cell surface. A-C Further examples of images and corresponding trajectories from TIRF-M time-lapse sequences acquired in three representative living CHO cells stained for actin (blue) and expressing single-molecule levels of SNAP-SSTR2 (green) and CLIP-FLNA (magenta), labeled with Alexa647-BG and TMR-BC dye, respectively. SSTR2 and FLNA trajectories are depicted

in green and magenta, respectively, whilst SSTR2−FLNA apparent interactions are represented by yellow trajectories. Scale bars, 1 μm.

Supplemental Video 1.

SSTR2 and FLNA during an apparent interaction on underlying actin fiber. Shown are individual SSTR2 (green) and FLNA (magenta) particles undergoing transient interactions over an actin fiber (blue) in a living CHO cell. Frames were acquired every 61.9 ms.

Supplemental Video 2.

SSTR2 and FLNA trajectories. Corresponding trajectories of individual SSTR2 (green) and FLNA (magenta) particles shown in Movie S1. The trajectories are colored in yellow during the apparent interaction.